IEEE Access
Multidisciplinary | Rapid Review | Open Access Journal

Received October 7, 2017, accepted December 27, 2017, date of publication January 18, 2018, date of current version March 19, 2018.

Digital Object Identifier 10.1109/ACCESS.2018.2794141

Multi-Modal Ship Target Image Smoothing Based on Adaptive Mean Shift

ZHAOYING LIU[1], XIANGZHI BAI[2,3,4], CHANGMING SUN[5], FUGEN ZHOU[2], AND YUJIAN LI[1]

[1]College of Computer Science, Beijing University of Technology, Beijing 100124, China
[2]Image Processing Center, Beihang University, Beijing 100191, China
[3]State Key Laboratory of Virtual Reality Technology and Systems, Beihang University, Beijing 100191, China
[4]Advanced Innovation Center for Biomedical Engineering, Beihang University, Beijing 100083, China
[5]CSIRO Data61, Epping, NSW 1710, Australia

Corresponding author: Xiangzhi Bai (jackybxz@buaa.edu.cn)

This work was supported in part by the National Natural Science Foundation of China under Grant U1736217, in part by the Program for New Century Excellent Talents in University under Grant NCET-13-0020, in part by the China Post-Doctoral Science Foundation funded Project under Grant 2015M580952, and in part by the project supported by Beijing Post-Doctoral Research Foundation under Grant 2016ZZ-24.

ABSTRACT In this paper, we propose an adaptive image smoothing method for infrared (IR) and visual ship target images, aiming to effectively suppress noise as well as preserve important target structures, thus benefiting image segmentation. First, by analyzing the specific features of ship target images, a block based method combining local region mean and standard deviation is developed to highlight ship target regions. It is helpful to distinguish the ship target region from the background. Then, by associating the range bandwidth with local image properties of the ship target region and the background region, we develop an adaptive range bandwidth mean shift filtering method for IR and visual ship target image smoothing. With this proposed method, we can obtain a small bandwidth for ship target region and a large one for the background region. Therefore, we can effectively smooth the background while preserving the details of the targets. Experimental results show that this method works well for IR and visual ship target images with different backgrounds. The method demonstrates superior performance for image smoothing and target preservation compared with the four well-known edge-preserving denoising methods, including the anisotropic diffusion filtering, the bilateral filtering, the propagation filtering, and the mean shift filtering with fixed range bandwidth.

INDEX TERMS Adaptive range bandwidth, mean shift filtering, edge-preservation, multi-modal image smoothing.

I. INTRODUCTION

Infrared (IR) and visual imaging sensors are widely used for maritime security and defense missions, such as harbor surveillance, traffic monitoring, and maritime search and rescue. [1]–[3]. However, due to the intrinsic limitations of imaging sensors and the variations of imaging scenario, ship target images are unavoidably corrupted by noises and have complex backgrounds, all these increase the difficulty of ship target detection and recognition in such applications [4]. Therefore, it is necessary to suppress the noises and complex backgrounds, and important target structures, such as edges, should be adequately preserved. Edge preserving filters can preserve the image details and local structures while removing the undesirable noises. Many edge preserving smoothing methods have been proposed [5]–[7], and they can be roughly divided into spatial domain based methods and transform domain based methods [8]. In this paper, we mainly focus on the spatial domain based filters. In the past decades, to preserve edges while denoising, many non-linear spatial domain filters have been proposed, such as median filtering [9], anisotropic diffusion filtering [10], bilateral filtering [12], and mean shift filtering [13].

As one of the most popular smoothing methods, the median filtering method is simple and computationally efficient. However, the traditional median filtering method may smooth some fine structures, and cause streaking effects [14]. In recent years, different types of median filtering have been proposed, such as progressive median filtering [15], adaptive switching median filtering [16], and decision based median filtering [17]. These techniques filter the image in two phases: first, an impulse detector is used to detect the pixels corrupted with impulse noise; then a filtering technique is used to filter

these corrupted pixels. By applying the detection and filtering techniques iteratively, all the noisy pixels can be detected and the corrupted pixels can be filtered [18].

Apart from the non-linear median filters, another popular edge preserving method is based on partial differential equations (PDEs) [11], such as the anisotropic diffusion filter [10]. However, the basic anisotropic diffusion model [10] is ill-posed and some artifacts such as staircasing and blocky effects usually happen. To avoid the artifacts, many improved methods have been developed [19], [20]. By applying a pre-processing step before anisotropic diffusion denoising, these improved methods can achieve better denoising results. However, these methods only consider the local gradient information of each pixel, important structures with low gradients would be over smoothed. Besides, they are implemented as an iterative process, the whole procedure are usually time consuming.

A good alternative to an iterative edge preserving method is bilateral filtering [12] which combines both intensity and spatial distances to preserve details. Recently, to achieve better edge preservation, a weighted method is proposed to balance the intensity difference and the geometric distance in determining the kernel coefficients [22]. Although bilateral filtering is non-iterative and the formulation is simple, the direct implementation is complex. Therefore, several strategies have been proposed to speed up the bilateral filtering [21]. Another issue concerning the bilateral filtering is that it may have the gradient reversal artifacts, and for images with low contrast, it will blur some important structures. Guided filter [23] can also be used as an edge-preserving filter like the bilateral filter, and it has better behaviors near edges with the ability of avoiding ringing artifacts [24]. Both bilateral and guided filters have been successfully applied to a variety of applications. However, the performance of these filters is affected by predefined pixel neighborhood regions, and it is difficult to determine these neighborhood parameters beforehand. To solve this problem, a propagation filter [25] was proposed. The propagation filter is able to smooth over images while preserving image context information, and this filter is based on the photometric relationship observed between image pixels. There are also some powerful non-local spatial domain methods, such as total variation method [26], [27], which is also widely applied in image restoration [28]; patch-based method [5], [29], which uses a weighted average of all similar patches in an image to take advantage of the repeating structures in the image; by considering a Gaussian probability model when collecting and averaging the similar patches, a non-local Bayes method was proposed in [30]. The non-local mean filter has been of interest because of its conceptual simplicity and effectiveness [31]. However, many of these denoising methods depend strongly on the noise models, assuming that the noise type and level are known in advance.

Similar to the bilateral filtering, mean shift filtering [13] is also an effective discontinuity preserving denoising method, which considers both intensity and spatial information. It has been widely used for image smoothing and segmentation [32], [33]. In the process of mean shift filtering, the performance is highly influenced by the bandwidth parameters, and it is difficult to find an optimal global bandwidth. To address this issue, various automatic bandwidth selection methods have been developed, such as cross-validation (CV) [34], plug-in (PI) [35], normal scale bandwidth [36], and smooth cross-validation (SCV) [37]. However, these methods only work well for certain data, and none of these fixed bandwidth selectors is uniformly preferable over the others [38]. It is reasonable that locally adaptive bandwidth may lead to good smoothing results [39], [40].

In this paper, an adaptive range bandwidth mean shift filtering method is developed for multi-modal ship target image smoothing. First, by analyzing the specific features of ship targets, local image properties are combined to distinguish the ship target region from the background. Then, by associating the range bandwidth of mean shift with local image properties of the ship target region and the background region, we propose an adaptive range bandwidth selection method. It can obtain a small bandwidth for a target region and a large one for the background; therefore, we can effectively smooth the background while preserving important target structures. It should be note that, in this work, we mainly focus on IR and visual images, as currently we just have these two types of images available. Nevertheless, the proposed method can be considered as a reference for dealing with other type of images.

The paper is structured as follows. In Section II, we introduce the detailed procedure of the proposed method. Section III demonstrates the experimental results on real IR and visual ship target images. Finally, conclusion is presented in Section IV.

II. THE PROPOSED METHOD

A. ADAPTIVE MEAN SHIFT ALGORITHMS

Mean shift smoothing algorithm is a robust feature space analysis approach [13]. In the process of mean shift filtering, the range bandwidth parameter h_r and the spatial bandwidth parameter h_s are important for the performance, especially h_r. To effectively smooth the background while preserving the target, it is reasonable to distinguish the target from the background and choose different bandwidths. In our previous work [40], we developed an adaptive mean shift filtering method for IR ship target image smoothing, which can effectively smooth the background and preserve detail structures of the IR ship targets. For more details about the mean shift, please refer to [13], [40]. In this work, we extended this method for multi-modal image smoothing. We mainly deal with IR and visual ship target images with sea and sky backgrounds, some examples are shown in Fig. 1. There are mainly two reasons why we made this extension. One is that in practical applications, e.g., ship target recognition, both the two modalities are commonly used and image denoising is always desirable to improve the image qualities. Dealing with

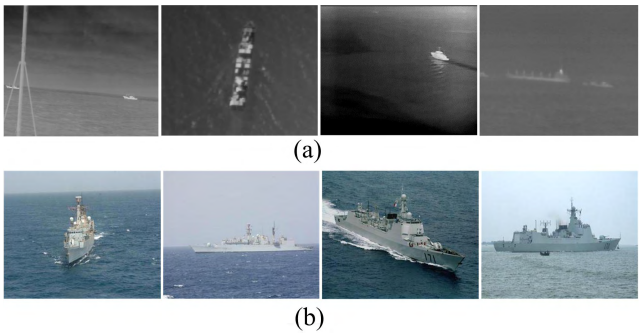

FIGURE 1. Samples of IR and visual ship target images. (a) IR ship target images; (b) Visual ship target images.

the two modalities in the same way is beneficial in reducing the complexity of algorithm design and hardware configuration. The other reason is that the proposed method is not restricted to image modalities. In other words, it is modality-independent. Dealing with both modalities may further show the good extendibility of the proposed method.

From Fig. 1 we can see that although different images have different backgrounds and ship targets, they still have something in common. Generally, there are mainly three regions: sky, ship target, and sea background, and the three regions have different intensity properties. Through the observation of the IR and visual ship target images, we find that they have the following three common properties:

Property 1: A ship target is a connected region with high visual saliency and high local contrast comparing with its surrounding backgrounds.

Property 2: The ship target region has relatively large standard deviation and gradient magnitude around the boundaries.

Property 3: For images with heavy sea clutters, the sea background region has a relatively large gradient magnitude but the standard deviation is small, because most of the wave clutters distribute in certain patterns.

Based on these three properties, we develop an adaptive range bandwidth selection method. Our goal is to select a large range bandwidth for the background region and a small one for the target region by using the local specific properties of the IR and visual ship target images. We express the range bandwidth h_r as a function f of the local region properties:

$$h_r(w_{xy}) = f(L_p(w_{xy})) \tag{1}$$

where w_{xy} is a sliding window centered at location (x, y); $L_p(w_{xy})$ represents the local region properties inside w_{xy}. In both modalities, the ship target and backgrounds are distinguishable, so we treat them in the same adaptive way. However, since the image acquisition process of the IR and visual images are different, the intensity distributions of the IR and visual images are different, the noise models are different. Therefore, we use different local region properties to calculate the range bandwidth for IR and visual images, seperately. The spatial bandwidth h_s is chosen

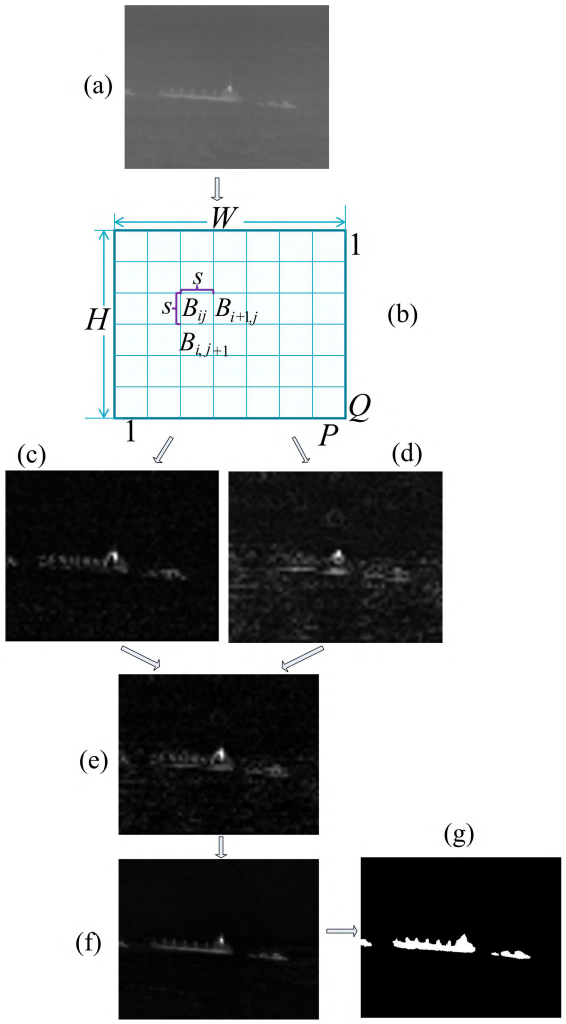

FIGURE 2. Ship target region detection. (a) An IR ship target image; (b) Block-based representation; (c) The mean difference map; (d) The standard deviation difference map; (e) The combined result; (f) The final saliency map; (g) The binary mask of the ship target region.

according to image dimensions as in [42], that is $h_s = \max\{4, \min\{H, W\}/100\}$. In the following subsections, the detection of the ship target region R_{target} and the background region $R_{background}$, and the calculations of the adaptive range bandwidth for IR and visual ship target images will be given in details.

1) BLOCK-BASED IR AND VISUAL SHIP TARGET REGION DETECTION METHOD

We use a block-based representation [41] to detect the ship target region both for the IR and visual images. Take an IR image as example, a brief introduction of the procedure is as follows. For more details about the salient target region detection please refer to [40]:

Firstly, given an IR image I (Fig. 2(a)) with size $W \times H$, we divide the image into $P \times Q$ non-overlapping blocks $\{B_{11}, \ldots, B_{1Q}; \ldots; B_{i1}, \ldots, B_{iQ}; \ldots; B_{P1}, \ldots, B_{PQ}\}$. B_{ij} is an $s \times s$ image block, $s = 11$, as shown in Fig. 2(b).

Secondly, we calculate the mean and standard deviation difference of the blocks. The mean difference is denoted as *mdf* (Fig. 2(c)), and the standard deviation difference is denoted as *sdf* (Fig. 2(d)).

$$mdf(B_{ij}) = \min\left((M_{i,j} - M_{i,j+1}), (M_{i,j} - M_{i+1,j})\right) \quad (2)$$

$$sdf(B_{ij}) = \max\left((S_{i,j} - S_{i,j+1}), (S_{i,j} - S_{i+1,j})\right) \quad (3)$$

where $M_{i,j}$ and $S_{i,j}$ are the mean and standard deviation values of the block B_{ij}, respectively.

Thirdly, the two maps are combined to highlight regions with greater differences comparing to its neighborhood, and the combined image I_c is shown in Fig. 2(e). To enhance the ship target, a row mean subtraction method is applied.

$$I_c(B_{ij}) = \sqrt{\left(mdf(B_{ij})\right)^2 + \left(sdf(B_{ij})\right)^2} \quad (4)$$

$$R_m(y) = \begin{cases} R_y - R_y^m, & \text{if } I_{med}(x,y) > R_y^m \\ 0, & \text{otherwise} \end{cases} \quad (5)$$

$$R_{cm}(y) = \begin{cases} R_y^c - R_y^{cm}, & \text{if } I_c(x,y) > R_y^{cm} \\ 0, & \text{otherwise} \end{cases} \quad (6)$$

where I_{med} is the smoothed result of the original image using a median filter. It is helpful to remove some noises initially. $R_y = \{R_{1,y}, R_{2,y}, \ldots, R_{x,y}, \ldots, R_{W,y}\}$ and $R_y^c = \{R_{1,y}^c, R_{2,y}^c, \ldots, R_{x,y}^c, \ldots, R_{W,y}^c\}$ are the pixel values vector of row y of image I_{med} and I_c respectively. $I_{med}(x, y)$ is the pixel value at position (x, y). R_y^m and R_y^{cm} are the mean values of R_y and R_y^c respectively.

Fourthly, the final region saliency map $Sal(x, y)$ (Fig. 2(f)) is obtained by combining the two row mean subtraction results, R_m and R_{cm}.

$$Sal(x, y) = R_m(x, y) + R_{cm}(x, y) \quad (7)$$

Finally, to identify the target region R_{target} and the background region $R_{background}$, a thresholding method is used to obtain the binarized mask, M_{sal}, as shown in Fig. 2(g).

$$M_{sal}(x, y) = \begin{cases} 1, & \text{if } Sal(x, y) \geq T_s \\ 0, & \text{otherwise} \end{cases} \quad (8)$$

Among the existing adaptive thresholding methods, mean and standard variance are widely used for threshold determination and have been proved to be effective. Therefore, we use flexible linear combination of mean and standard variance to determine the thresholds. The threshold T_s is obtained as

$$T_s = \mu_s + \gamma\sigma_s \quad (9)$$

where μ_s and σ_s are the mean and standard deviation values of the salient map *Sal*; γ is a control parameter. Currently, the gamma parameter used are set in a heuristic way, which is set to 5 in the implementation. The binarized mask M_{sal} is used to label the target region R_{target} and the background region $R_{background}$. If $M_{sal}(x, y) = 1$, then $(x, y) \in R_{target}$, $R_{target}(x, y) = 1$, otherwise $R_{target}(x, y) = 0$; if $M_{sal}(x, y) = 0$, then $(x, y) \in R_{background}$, $R_{background}(x, y) = 1$, otherwise $R_{background}(x, y) = 0$.

B. RANGE BANDWIDTH CALCULATION FOR IR SHIP TARGET IMAGE

From Fig. 1(a) we can see that just as stated in *Property 1* and *Property 2*, an IR ship target has higher visual saliency and higher local contrast than its surrounding backgrounds. Standard deviation and gradient magnitude around the boundaries are important features for distinguishing the background and the target regions. For the ship target region, local standard deviation and gradient magnitude around the boundaries are relatively large; while for the sea wave clutters, the gradient magnitude is relatively large but the standard deviation is small; for the other noises, they are relatively random distributed. Therefore, to preserve the ship target region, the range bandwidth is associated with the local standard deviation, the local gradient magnitude, and the region saliency. For each pixel I_{xy} in I at location (x, y), $x = 1, \ldots, W$; $y = 1, \ldots, H$, a sliding window w_{xy} with size $d \times d$ centered at (x, y) is used to calculate the local standard deviation and the local magnitude of the gradient; similarly, for each pixel $Sal_{x,y}$ in the saliency map *Sal*, a sliding widow with the same size is used to calculate the local region saliency. To be consistent with the mean shift smoothing process, the window size used here is the same as the mean shift, that is $d = (2 \times h_s + 1)$. The range bandwidth of window w_{xy}, $h_r^{IR}(w_{xy})$, which is denoted as h_r^{IR}, is obtained as

$$h_r^{IR} = \begin{cases} 3h_{r0}, & \text{if } L_{std}^{IR} = 0 \,\|\, L_{grad}^{IR} = 0 \\ h_{r0}/L_p^{IR}, & \text{else if } (x, y) \in R_{target} \\ 2h_{r0}/L_p^{IR}, & \text{else } (x, y) \in R_{background} \end{cases} \quad (10)$$

where $L_p^{IR} = L_{std}^{IR} \times L_{grad}^{IR} \times L_{sal}^{IR} + 1$; L_{std}^{IR}, L_{grad}^{IR}, and L_{sal}^{IR} are the local standard deviation, local magnitude of the gradient, and local saliency of the processing kernel window w_{xy} respectively. h_{r0} is a fixed initial value of h_r, which is set to 10. For regions with local standard deviation or local magnitude of the gradient being zero, we just smooth them using a fixed range bandwidth. With expression (10), we aim to adaptively select proper range bandwidth for the ship target region and background region.

Proposition 1: If a pixel I_{xy} belongs to the ship target regions, i.e., $I_{xy} \in R_{target}$, the range bandwidth $h_r < h_{r0}$.

Proof: For the pixel I_{xy} which belongs to the ship target region, according to *Property 1* and *Property 2*, the local standard deviation (L_{std}^{IR}), magnitude of the gradient (L_{grad}^{IR}), and local saliency (L_{sal}^{IR}) will be relatively large, especially when the pixel is close to an edge. In general, for the test IR images, $L_{std}^{IR} > 5$, $L_{grad}^{IR} > 20$, and $L_{sal}^{IR} > 0.2$. By multiplying the L_{std}^{IR}, the L_{grad}^{IR}, and the L_{sal}^{IR}, we will obtain a relatively large L_p^{IR}, that is $L_p^{IR} = L_{std}^{IR} \times L_{grad}^{IR} \times L_{sal}^{IR} + 1 > 20$. With a fixed numerator h_{r0}, the value of a fraction is inversely proportional to that of the denominator L_p^{IR}, therefore, we will obtain a range bandwidth $h_r < h_{r0}$. In fact, h_r is much smaller than the h_{r0}. Similarly, we can prove that for a pixel belonging to the background region, a range bandwidth $h_r > h_{r0}$ will be obtained.

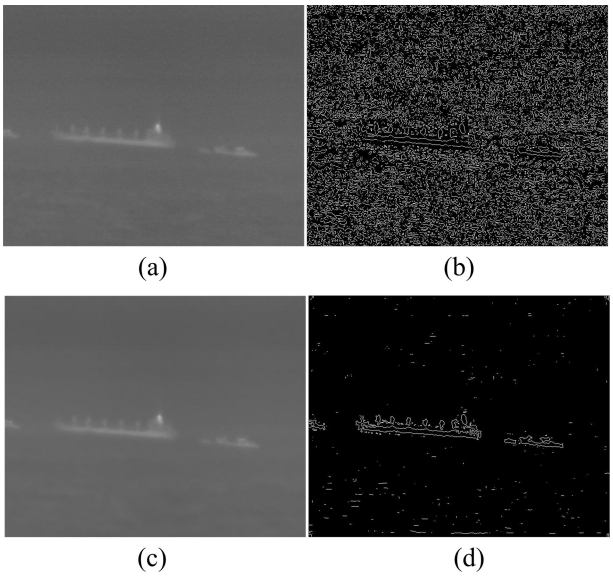

FIGURE 3. IR image smoothing result. (a) The original IR image; (b) The edge map of the original IR image; (c) The smoothed IR image; (d) The edge map of the smoothed IR image.

Consequently, by associating the range bandwidth with the local standard deviation, local gradient magnitude, and local region saliency, we can properly adjust the range bandwidth according to different regions, achieving the purpose of effectively smoothing the background while preserving the ship target. One example of the smoothing results is shown in Fig. 3. To illustrate the effect of image denoising and edge preservation, we detect the edges using the Laplacian of Gaussian (LoG) operator and make a comparison with the unsmoothed image. Fig. 3(b) shows the edge map of the original unsmoothed IR image, and Fig. 3(d) shows the edge map of the smoothed image.

Fig. 3 demonstrates that with the proposed adaptive range bandwidth mean shift filtering method, we can successfully smooth the IR image. From Fig. 3(b), the edge map of the original IR image, we can see that the original image is degraded with heavy background noises. After using the proposed smoothing method, we can see clearly that the IR image is well smoothed (Fig. 3(c)), and most of the background noises have been effectively suppressed (Fig. 3(d)).

C. RANGE BANDWIDTH CALCULATION FOR VISUAL SHIP TARGET IMAGE

As shown in Fig. 1, the visual ship target images are RGB (Red, Green, Blue) color images containing a big ship target with sea-sky backgrounds. The ship target is a connected region with salient contour information, and the sea background is complex with heavy sea wave clutters and noises. To obtain grey-level images, an RGB to HSI (Hue, Saturation, Intensity) color space conversion is performed on the visual image [43]. Compared with the RGB color model, the HSI color model represents colors similar to how the human eye senses colors. Therefore, it is more intuitive and efficient for image processing applications.

After converting to the HSI color space, we perform the mean shift filtering on the intensity component, and by transforming the smoothing result to the RGB color space we obtain the final smoothing result. Given an intensity component I_n, as with the IR image, we calculate the local standard deviation map S_m and the local gradient magnitude map G_m for each pixel I_{nxy} in I_n at location (x, y), $x = 1, \ldots, W; y = 1, \ldots, H$ using a sliding window w_{xy} with size $d \times d$ centered at (x, y) , as shown in Fig. 4.

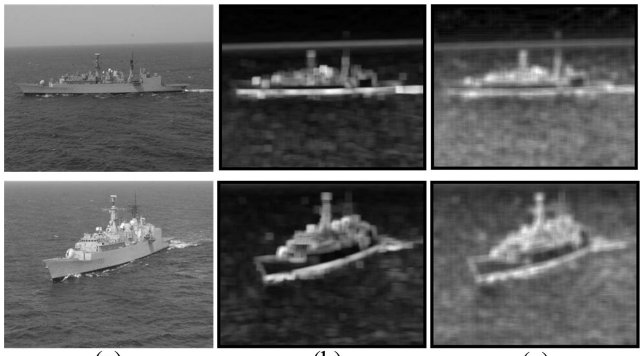

FIGURE 4. Local properties of visual ship target images. (a) Intensity component of the original visual images (*I*); (b) The images of local standard deviation (*S*); (c) The images of local gradient magnitude (*G*).

We can see from Fig. 4 that the ship target region has a relatively large local standard deviation and a high gradient magnitude around the boundaries; while the sea background region has a relatively large gradient magnitude but the standard deviation is small, especially those waves which are far away from the ship target, just as stated in *Property 3*. Therefore, local region standard deviation and gradient are used to calculate the range bandwidth, as expressed below:

$$h_r^V = \begin{cases} 3h_{r0}, & \text{if } L_{std}^V = 0 \| L_{grad}^V = 0 \\ h_{r0} \cdot L_p^V, & \text{else if } \in R_{target} \\ h_{r0} \cdot L_p^V, & \text{else } (x, y) \in R_{background} \end{cases} \tag{11}$$

where $L_p^V = \left| L_{grad}^V - L_{std}^V \right| \cdot L_{grad}^V / (L_{std}^V + 0.1)$, and the L_{std}^V and L_{grad}^V represent the local standard deviation and gradient magnitude in the sliding window w_{xy} respectively.

According to the analysis of the local region properties of the visual ship images (Fig. 4), we can obtain the following proposition and prove that with expression (11), a large range bandwidth h_r will be obtained for the sea clutters and a small one will be obtained for the ship target region.

Proposition 2: If a pixel I_{xy} belongs to sea background regions, that is $I_{xy} \in R_{background}$, the range bandwidth $h_r > h_{r0}$.

Proof: If pixel I_{xy} belongs to the sea background clusters, the magnitude of the gradient (L_{grad}^V) will be a relatively large value, and the local standard deviation (L_{std}^V) will be a relative small one (*Property 3*). Generally, for the tested visual images, $L_{grad}^V > 15$, and $L_{std}^V < 5$. With a large numerator L_{grad}^V and a small denominator L_{std}^V, the fraction L_{grad}^V / L_{std}^V

is greater than 1, e.g., $L^V_{grad}/L^V_{std} > 15/5 > 1$. On the other hand, if we subtract L^V_{std} from L^V_{grad}, we can still obtain a relatively large value, e.g., $L^V_{grad} - L^V_{std} > 15 - 5 = 10$. Therefore, through multiplying the two expressions, that is $(L^V_p = \left|L^V_{grad} - L^V_{std}\right| \cdot L^V_{grad}/\left(L^V_{std} + 0.1\right) > 10)$, we obtain a relatively large L^V_p. Therefore, a $h_r > h_{r0}$ is obtained $(h_r = h_{r0} \cdot L^V_p > 10h_{r0})$. Similarly, we can prove that for a pixel belonging to the target region, a $h_r < h_{r0}$ will be obtained.

Consequently, it can be concluded that by associating the range bandwidth with the local standard deviation and local gradient magnitude, we can properly adjust the range bandwidth according to different regions, achieving the purpose of effectively suppress the complex sea background while preserving the ship target. Fig. 5 shows a smoothing result of the visual ship target images using the proposed method. To illustrate the effect of image denoising and complex sea background suppression, we also detect the edges using the LoG operator and make a comparison with the unsmoothed image. Fig. 5(a) shows the intensity component of the original image, Fig. 5(b) is the edges extracted using LoG, Fig. 5(c) shows the smoothed image, and Fig. 5(d) is the corresponding edges extracted using LoG.

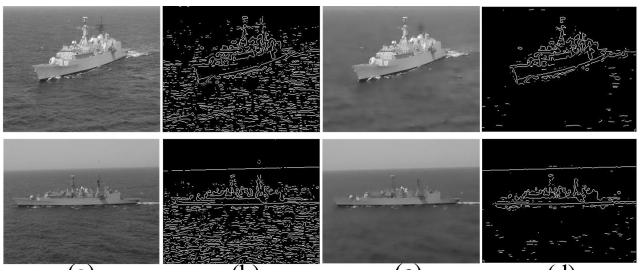

FIGURE 5. Visual ship target image smoothing result. (a) Intensity component of the original visual images; (b) The edge map of the original visual images; (c) The smoothed visual images; (d) The edge map of the smoothed visual images.

From Fig. 5 we can see that, with the proposed smoothing method, the images can be effectively smoothed. By comparing with the edge images shown in Fig. 5(b) and Fig. 5(d), we can clearly see that most of the edges caused by sea wave clutters have been removed while the details of ship target have been well preserved.

III. EXPERIMENTAL RESULTS AND APPLICATIONS

A. IMAGE SMOOTHING RESULTS

The proposed method is tested on an image dataset supplied by co-researchers, including 310 real IR ship target images and 500 real visual images with different ship targets and backgrounds. The IR images were acquired by fixed ship-borne cameras with different backgrounds, which are commonly used for maritime surveillance. Parts of the visual images are downloaded from the publicly available website (http://www.cnss.com.cn/). The image size ranges from 320 × 256 to 720 × 576 pixels for the IR ship target images,

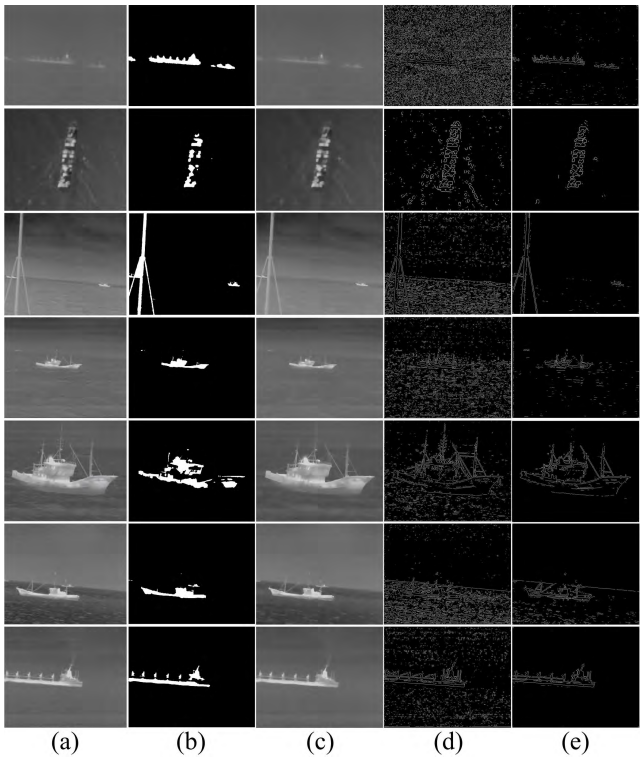

FIGURE 6. IR image smoothing results. (a) The original IR images; (b) The target detection results; (c) The smoothed IR images; (d) The edge map of the original IR images; (e) The edge map of the smoothed images.

and from 320 × 256 to 1025 × 768 pixels for the visual ship target images. We tested the proposed method using xed parameters given in Section II. The experiments were implemented using MATLAB R2012b, using an Intel(R) Core(TM) i5-2400 processor, 3.10 GHz CPU, with 4.00 GB RAM. Parts of the experimental results are shown in Fig. 6 and Fig. 7.

Fig. 6(a) shows the original IR images, Fig. 6(b) shows the target region detection results using the proposed block-based method, Fig. 6(c) shows the smoothed images, Fig. 6(d) shows the edge maps of the original images, and Fig. 6(e) shows the edge maps of the smoothed images. Fig. 7(a) is the original visual images, Fig. 7(b) shows the target region detection results, Fig. 7(c) shows the smoothed images, Fig. 7(d) shows the edge maps of the original images, and Fig. 7(e) shows the edge map of the smoothed images.

From Fig. 6(c) and Fig. 7(c) we can see that the proposed method works well for both IR and visual images with different ship targets and backgrounds. By comparing the edge maps of the original images (Fig. 6(d) and Fig. 7(d)) and the edge maps of the smoothed images (Fig. 6(e) and Fig. 7(e)), we can clearly see that all the images are well smoothed, most of the background noises are removed, and the ship target regions are well preserved.

B. COMPARISON RESULTS

1) VISUAL COMPARISON

To illustrate the effectiveness of the proposed method, comparisons are made with four other methods: the anisotropic

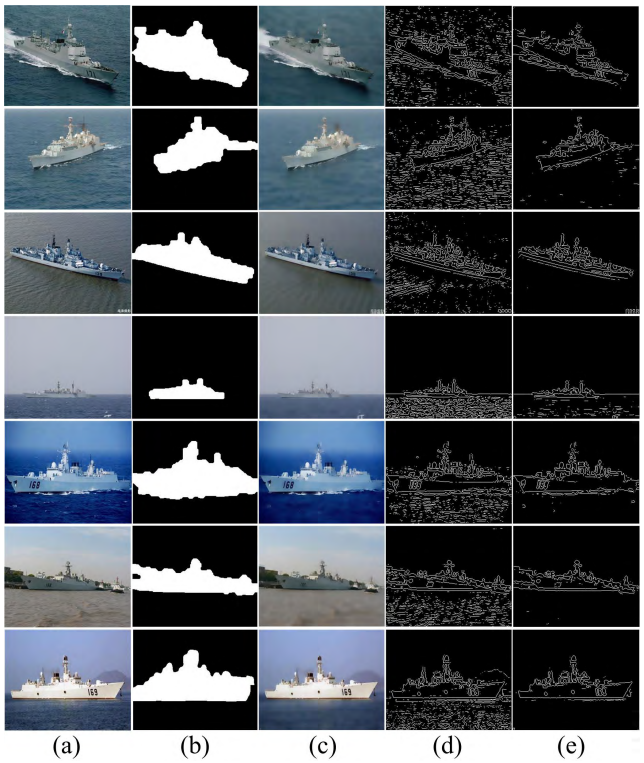

FIGURE 7. Visual image smoothing results. (a) The original visual images; (b) The target detection results; (c) The smoothed visual images; (d) The edge maps of the original visual images; (e) The edge maps of the smoothed images.

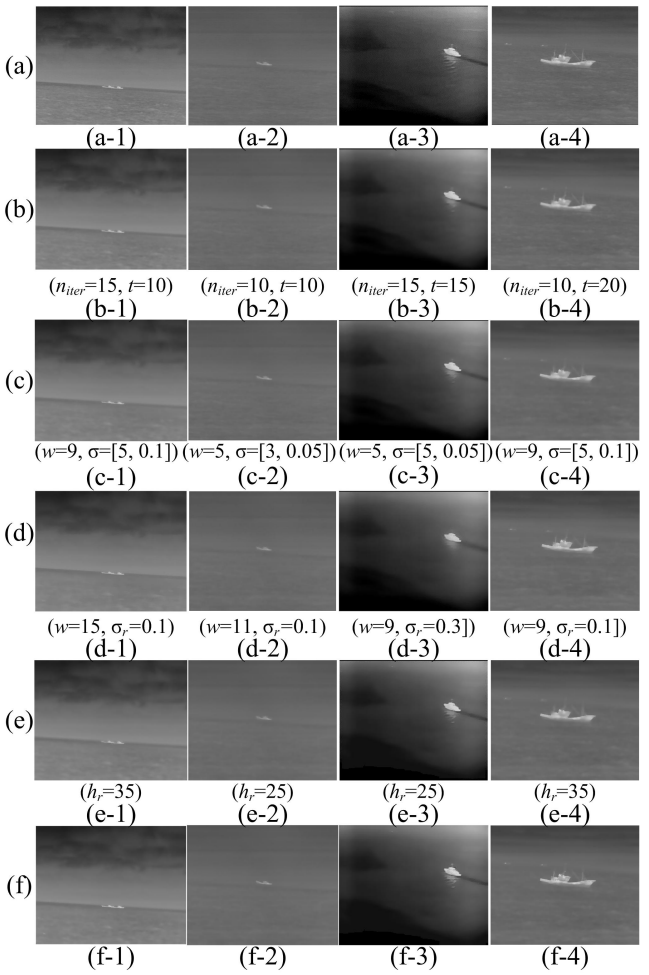

FIGURE 8. Comparison results of IR images with different backgrounds. (a) The original IR images; (b) Results of anisotropic diffusion filtering with two parameters (n_{iter}, t); (c) Results of bilateral filtering with two parameters (w; σ); (d) Results of the propagation filtering with parameters (w; σ_r); (e) Results of mean shift filtering with fixed range bandwidth (h_r); (f) Results of the proposed method.

diffusion filtering (Anisotropic) [10], the bilateral filtering (Bilateral) [22], the propagation filtering [25], and the mean shift filtering with fixed range bandwidth (Mean shift) [13]. The reason why we choose these four methods is that they are commonly used edge-preserving denoising methods for different types of noises. In fact, as the IR and visual images used in our experiment were obtained from practical applications and the noises are complex, it is difficult to build a precise noise model. Therefore, in our experiments, there is no restriction to the type of noises. To make the comparison reasonable, we tried to obtain the best possible result by tuning the relevant parameters, including the number of iteration n_{iter} and the gradient modulus threshold t used in the anisotropic diffusion filtering; the half-size of the filtering window w and the standard deviations $\sigma = [\sigma_s, \sigma_r]$ used in the bilateral filtering, the window radius w and the standard deviation σ_r of the propagation filtering, and the range bandwidth h_r of the mean shift filtering. Comparison results on different IR and visual images are shown in Fig. 8 and Fig. 9.

Fig. 8 shows the comparison results of IR images with different backgrounds and ship targets, such as images with heavy sea clutters, low contrasts, uneven high contrast backgrounds, and multiple different sized ship targets. For the IR images with complex backgrounds (Fig. 8(a-1)), the corresponding smoothing results using the listed methods (the Anisotropic (Fig. 8(b-1)), the Bilateral (Fig. 8(c-1)), the propagation filtering (Fig. 8(d-1)), the Mean shift (Fig. 8(e-1)), and the proposed method (Fig. 8(f-1)) are shown in the first row of Fig. 8(b)-Fig. 8(f). We can see that the performances of the anisotropic diffusion filtering (Fig. 8(b-1)) and the bilateral filtering (Fig. 8(c-1)) methods are similar. Both methods can smooth some background noises. However, they are unable to completely suppress the heavy sea clutters, and the edges of the ship target region are blurred. Fig. 8(d-1) shows the result of the propagation filter, from which we can see that with reasonable parameters, the propagation filter achieves a better denoising performance than the bilateral filter, the edges of the ship target are well preserved. From Fig. 8(e-1), we can see that with the fixed range bandwidth, the mean shift filtering method can effectively suppress the heavy sea clutters; however, the boundaries of the ship target are also smoothed. With a smaller fixed range bandwidth, the ship target region can be well preserved, but the background cannot be well suppressed. Therefore, for the mean shift filtering method with fixed bandwidth, it is

difficult to choose a proper bandwidth. Note that in our experiments, we tried to choose a range bandwidth that can balance the smoothing of background and the preservation of the target region. Fig. 8(f-1) shows that with the proposed method, we can effectively suppress the complex sea clutters around the ship target region, and also preserve the ship target region. Therefore, for IR images with complex sea clutters, the proposed method produces better results than the others.

For IR images with a small ship target embedded in sky and sea backgrounds with low contrast (Fig. 8(a-2)), the corresponding smoothing results are listed in the second row. We can see that the anisotropic diffusion filtering method (Fig. 8(b-2)) does not work well for this image. The ship target is smoothed but the sea background is not well suppressed. From Fig. 8(b-2) to Fig. 8(d-2), we can see that both the bilateral filter and the propagation filter have better performances than the anisotropic diffusion filter. They can effectively smooth the sea background and preserve most of the ship target region from being smoothed. From Fig. 8(e-2) we can see that the original mean shift filtering with fixed range bandwidth obtains a good smoothing result. It can effectively suppress the sea background while preserve the ship target. However, edges in the left parts of the ship target are blurred. Compared with the mean shift method with fixed bandwidth, the proposed adaptive method can preserve all the edges of the ship target and effectively smooth the background. The results listed from Fig. 8(b-2) to Fig. 8(f-2) indicate that the adaptive range bandwidth selection method is effective. With the proposed method, we can automatically choose good range bandwidths for image smoothing.

For IR images with high contrast and uneven background (Fig. 8(a-3)), the corresponding smoothing results are listed in the third row. From Fig. 8(a-3) we can see that the IR image is degraded with background noises. Fig. 8(b-3)-Fig. 8(f-3) demonstrate that all the listed methods can successfully remove the background noises and obtain a smoothed image. The results of the anisotropic diffusion filtering (Fig. 8(b-3)), the bilateral filtering (Fig. 8(c-3)), and the propagation filtering (Fig. 8(d-3)) are comparable. Although all the four methods can effectively smooth the background, the upper part structure of the ship target are seriously blurred, especially when using the anisotropic diffusion filtering and the propagation filtering methods. The performance of the mean shift with fixed range bandwidth and the proposed method are similar (Fig. 8(e-3) and Fig. 8(f-3)). They can effectively smooth the background while preserving the ship target structures. The results also validate the effectiveness of the proposed adaptive range bandwidth selection method. With the proposed range bandwidth selection method, we can automatically obtain a proper range bandwidth for image smoothing.

For IR images containing multiple ship targets with different sizes (Fig. 8(a-4)), we can see from Fig. 8(b-4) that the anisotropic diffusion filtering method cannot successfully preserve the ship targets region, and the whole images are blurred. From the result of the bilateral filtering (Fig. 8(c-4)) we can see that the bilateral filtering performs better than the anisotropic diffusion filtering method. The bilateral filtering method can suppress most of the sea background clutters and most of the large ship target regions are well preserved. However, the two small ship targets are severely blurred, and there are still slightly over smoothing around the boundaries of the large ship target. Fig. 8(d-4) demonstrates that the propagation filtering method can well overcome the problem of the bilateral filtering. It can effectively suppress the background and preserve the details of the two small ship targets. Fig. 8(e-4) and Fig. 8(f-4) show the results of mean shift filtering with fixed range bandwidth and the proposed adaptive range bandwidth. From Fig. 8(e-4) and Fig. 8(f-4) we can see that both methods can effectively suppress the backgrounds. However, the two small ship targets are also over smoothed, and some details of the largest ship target are also blurred. For this image, although none of the listed methods can obtain excellent performance, comparing with the other methods, the proposed method still obtains the best result. The proposed method can preserve most of the details of all the ship targets while effectively smoothing the background.

Fig. 9 shows the comparison results of visual images with different backgrounds and ship targets. From Fig. 9(b) we can see that the anisotropic diffusion filtering method can successfully smooth all the backgrounds, even for the image with heavy clutters (Fig. 9(b-3)). However, this method usually causes blurring, especially for images with low target and background contrasts (Fig. 9(b-1)). In contrast, the bilateral filtering method demonstrates a better performance than the anisotropic diffusion filtering (Fig. 9(c-1), Fig. 9(c-2)). The bilateral filtering method can preserve details of the ship targets. However, for images with heavy clutters (Fig. 9(c-3), Fig. 9(c-4)), parts of the background are not well suppressed. Fig. 9(d) demonstrates that the propagation filtering method works well for the visual images. By choosing reasonable parameters, this method can successfully smooth the backgrounds and preserve the ship targets. Even for images with heavy clutters, we can still obtain well smoothed backgrounds (Fig. 9(d-3), Fig. 9(d-4)). We can see from Fig. 9(e) and Fig. 9(f) that the performances of the original mean shift filtering with fixed range bandwidth and the proposed adaptive range bandwidth are similar. Both the two methods can effectively smooth the backgrounds and preserve most of the ship target structures. By comparing the two pair of images Fig. 9(e-1) and Fig. 9(f-1), Fig. 9(e-4) and Fig. 9(f-4) in details, we can see that the proposed mean shift filtering method with adaptive range bandwidth obtains better results in edge preservation.

From the comparison results in Figs. 8 and Fig. 9 we can see that in all cases the proposed method outperforms the other competitive methods. For some images, the results between the original non-adaptive and proposed adaptive mean shift are not fundamentally different. In fact, that is just a good verification of the proposed method. With the proposed adaptive range bandwidth selection method, we can

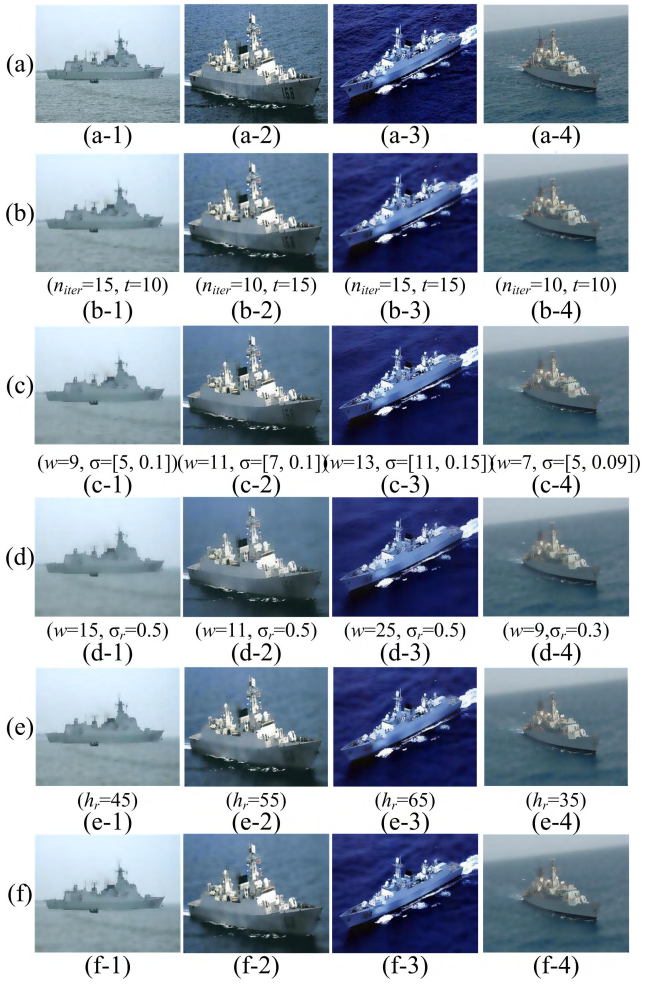

FIGURE 9. Comparison results of different visual images. (a) The original visual images; (b) Results of the anisotropic diffusion filtering with two parameters (n_{iter}, t); (c) Results of the bilateral filtering with two parameters (w; σ); (d) Results of the propagation filtering with parameters (w; σ_r); (e) Results of mean shift filtering with fixed range bandwidth (h_r); (f) Results of the proposed method.

obtain equivalent or even better results compared with the manually selection method. Therefore, it can be concluded that the proposed adaptive range bandwidth mean shift filtering is effective. It demonstrates a superior performance for both IR and visual ship target image smoothing.

2) QUANTITATIVE COMPARISON

To further verify the effectiveness of the proposed method, quantitative evaluation is performed. As reference standard images are unavailable, quantitative evaluation with references can not be used. In this paper, we take three no-reference measures and the processing time for performance analysis. The three measures are local phase coherence - sharpness index (LPC-SI) [44], edge based contrast measurement (EBCM) [45], and speckle suppression and mean preservation index (SMPI) [46].

The LPC-SI measures the sharpness of a test denoised image without referencing the original image. LPC-SI being 1 means very sharp, and 0 means very blurred. The EBCM measures the local contrast of each pixel, and a higher value of EBCM indicates a higher local contrast associated with each pixel in a given neighborhood. The SMPI measures speckle suppression and mean preservation capabilities of denoising techniques. A larger SMPI value means a better performance of the filter. The quantitative evaluation results on the IR and visual images with the average LPC-SI, EBCM, SMPI, and the average processing time are shown in Table 1.

TABLE 1. Quantitative evaluation results.

IR images				
Method	LPC-SI	EBCM	SMPI	time(s)
Anisotropic	0.675	0.347	0.0137	**0.1783**
Bilateral	0.636	0.3789	0.0146	2.4511
Propagation	0.7082	0.3909	0.1802	3.8672
Mean shift	0.6889	0.4168	0.2007	3.0509
Proposed method	**0.7384**	**0.59**	**0.2117**	3.7121
Visual images				
Method	LPC-SI	EBCM	SMPI	time(s)
Anisotropic	0.8857	0.6593	0.0419	**0.1253**
Bilateral	0.8774	0.6281	0.1777	1.4527
Propagation	0.8901	**0.6793**	0.1451	1.9644
Mean shift	0.8837	0.6321	0.0848	1.5164
Proposed method	**0.8906**	0.6773	**1.0395**	2.0836

From Table 1, we can see that in terms of LCP-SI, EBCM, and SMPI, the proposed method gives better performance than the other four methods. The proposed method obtains a higher average LCP-SI, a higher average EBMC, and a higher average SMPI, indicating that the proposed method is effective for noise suppression and can obtain a smoothed image with high local contrast and sharpness. The average processing time shown in Table 1 demonstrates that the anisotropic diffusion filtering method is the fastest one among the listed methods. It is much faster than the other listed four methods. The bilateral filtering method is much slower than the anisotropic diffusion filtering method, but it is faster than the propagation filtering, the mean shift filtering, and the proposed methods both for the IR and visual image smoothing. The computing time of the propagation filtering method and the proposed method are comparable. For the visual images, the propagation filtering method is a bit faster than the proposed method, while for the IR images, our proposed method is faster than the propagation filtering method. In the proposed method, we add a target detection procedure before the smoothing and local region properties computations during the smoothing procedure. These computations increase the computing complexity of the algorithm, thus the proposed method takes more computing time than the original mean shift method. In future work, parallel computation methods will be studied to improve the efficiency.

C. APPLICATIONS

Image smoothing is an important preprocessing procedure for a variety of applications in image processing and computer vision. To verify the effectiveness of the proposed method, we apply our adaptive mean shift filtering results to two applications, ship target image segmentation and saliency detection. For each application, we compare the results obtained by the anisotropic diffusion filtering [10], the bilateral filtering [22], the propagation filtering [25], the mean shift filtering with fixed range bandwidth [13], and the proposed adaptive mean shift filtering method.

1) IMAGE SEGMENTATION

Ship target image segmentation aims at partitioning the image into non-intersecting regions with each region being homogeneous, so that in the resulting image the background and the ship target regions are separated. Edge preserving image smoothing is useful for improving the performance of image segmentation. To demonstrate the effectiveness of the proposed method, we apply the smoothed image of our adaptive mean shift filtering to IR and visual ship target image segmentation, and compare the segmentation outputs produced by using the smoothed images of the anisotropic diffusion filtering, the bilateral filtering, the propagation filtering, and the mean shift filtering with fixed range bandwidth. For IR images, we use the entropy based thresholding method [47] which is simple and commonly used for IR image segmentation. For visual images, we use the random walker image segmentation method [48] which is an effective interactive image segmentation method. Fig. 10 and Fig. 11 show the segmentation results on IR and visual ship target images. To obtain more detailed quantitative evaluations, we choose two measures for performance analysis, misclassification error (ME) and relative foreground area error (RAE), please refer to [49] for the detailed definitions. Note that as there was no ground truth publicly available, we constructed 100 visual ship target images and 200 infrared ship target images as reference ground truth for segmentation. The quantitative evaluation results in terms of the misclassification error (ME) and relative foreground area error (RAE) are demonstrated in Table 2. For fair comparisons, we chose the parameters which can obtain the best possible segmentation results.

From Fig. 10(a), we can see that with low contrasts and heavy sea clutters, the original IR images are difficult to be segmented. Fig. 10(b) demonstrates that after being smoothed using the anisotropic filtering method, some noises can be effectively suppressed. However, the ship targets can still not be successfully separated from the backgrounds. Contrast to the anisotropic filtering method, the bilateral filtering method can effectively suppress the background and separate the background from the ship targets. Unfortunately, this method causes over smoothing. Parts of the ship target are classified as backgrounds and being removed during the segmentation procedure, as shown in Fig. 10(c). Fig. 10(d) shows the segmentation results of the images smoothed using the propagation filtering method, from which we can see that the IR

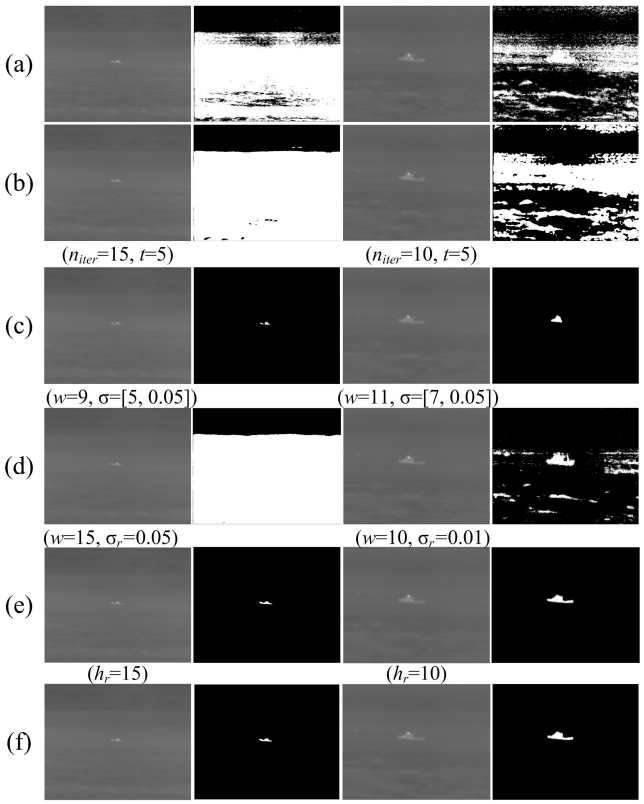

FIGURE 10. IR image segmentation results. Segmentation results of: (a) The original IR images; (b) The smoothed results of the anisotropic diffusion filtering, (n_{iter}, t); (c) The smoothed results of the bilateral filtering, (w; σ); (d) The smoothed results of the propagation filtering, (w; σ_r); (e) The smoothed results of the mean shift filtering with fixed range bandwidth, (h_r); (f) The smoothed results of the proposed method.

ship target images are well smoothed. However, for the image with small ship target and low contrast, the smoothed image obtained using this filtering method can not be successfully segmented. Fig. 10(e) and Fig. 10(f) demonstrate the segmentation results of the smoothed images obtained using the mean shift filtering with fixed bandwidth and the proposed adaptive bandwidth mean shift filtering method respectively. We can clearly see that the ship targets are effectively segmented, achieving satisfying results. After image smoothing using these two methods, we can successfully suppress the backgrounds and preserve the ship targets, making it much easier to separate the ship targets from the backgrounds. From Figure 10 we can see that, as the ship target is relatively small and the contrast is low, it is difficult to converge to a satisfactory result. The proposed edge-preserving smoothing method is helpful in reducing the difficulty of convergence.

Fig. 11 demonstrates the segmentation results of the visual ship target images. The green and blue spots denote the seeds of the foreground and the background respectively. The seeds are selected manually according to each original visual image. They are used for all the compared filtered images. The smoothed images are overlaid with their corresponding contours of the segmented ship targets, marked

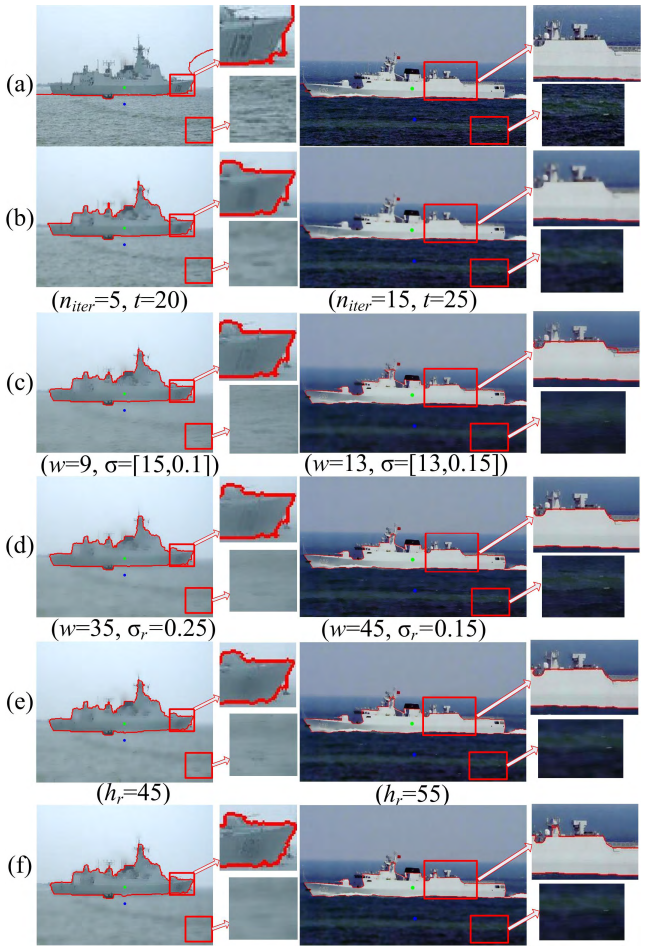

FIGURE 11. Visual image segmentation results. Segmentation results of: (a) The original visual images; (b) The smoothed results of the anisotropic diffusion filtering, (n_{iter}, t); (c) The smoothed results of the bilateral filtering, (w; σ); (d) The smoothed results of the propagation filtering, (w; σ_r); (e) The smoothed results of the mean shift filtering with fixed range bandwidth, (h_r); (f) The smoothed results of the proposed method.

with red color. To demonstrate the segmentation results more clearly, we enlarged parts of the targets and backgrounds. The corresponding patches are indicated with red arrows. From this figure, we can see that except for the anisotropic filtering method (as shown in the right column of Fig. 11(b)), most of the listed smoothing methods can improve the performance of the random walker segmentation method. By comparing the segmentation details of local enlarged patches of Fig. 11(a) - Fig. 11(f), we can see that the segmented contours of the smoothed images obtained using the proposed method are more consistent with the real ship targets, and the backgrounds are well smoothed.

From Table 2 we can see that the proposed method obtain the lowest average ME and RAE, especially for the IR images, our method achieves a superior performance comparing with the other four methods. Therefore, from Fig. 10, Fig. 11 and Table 2, we can verify that our proposed filtering method can be applied to improve the performance of IR and visual ship target image segmentation.

TABLE 2. Quantitative evaluation results of the segmentation application.

IR images		
Method	ME	RAE
Anisotropic	0.2815	0.7834
Bilateral	0.2786	0.7816
Propagation	0.2795	0.7817
Mean shift	0.2751	0.7726
Proposed method	**0.1310**	**0.6933**
Visual images		
Method	ME	RAE
Anisotropic	0.2439	0.5637
Bilateral	0.2877	0.5965
Propagation	0.2434	0.6184
Mean shift	0.2353	0.5663
Proposed method	**0.1736**	**0.5607**

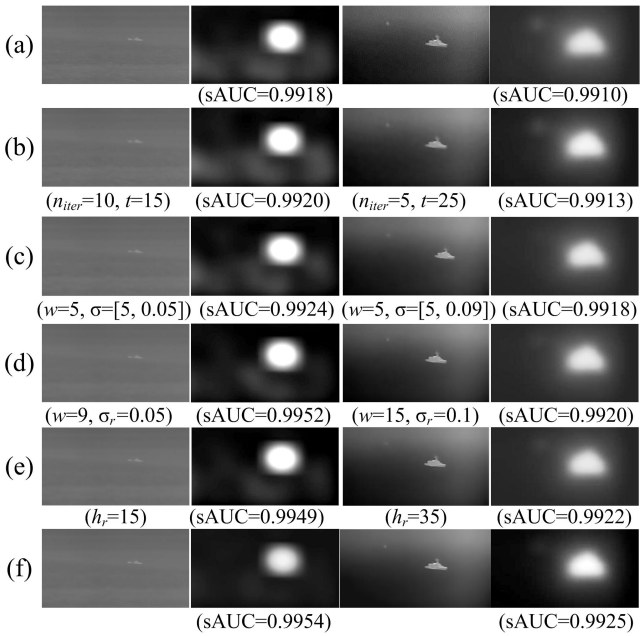

FIGURE 12. IR image saliency detection results. Saliency map of: (a) The original IR images; (b) The smoothed results of the anisotropic diffusion filtering, (n_{iter}, t); (c) The smoothed results of the bilateral filtering, (w; σ); (d) The smoothed results of the propagation filtering, (w; σ_r); (e) The smoothed results of the mean shift filtering with fixed range bandwidth, (h_r); (f) The smoothed images obtained using the proposed method.

2) SALIENCY DETECTION

Saliency detection is basically a process that highlighting visually salient regions in an image by detecting scene regions different from their surroundings [50]. It has recently drawn extensive attentions and a good saliency detection result is beneficial in many applications, such as image segmentation, object recognition, and target tracking. The task of saliency detection in its essence is a segmentation problem but not the same with the traditional image segmentation. Many

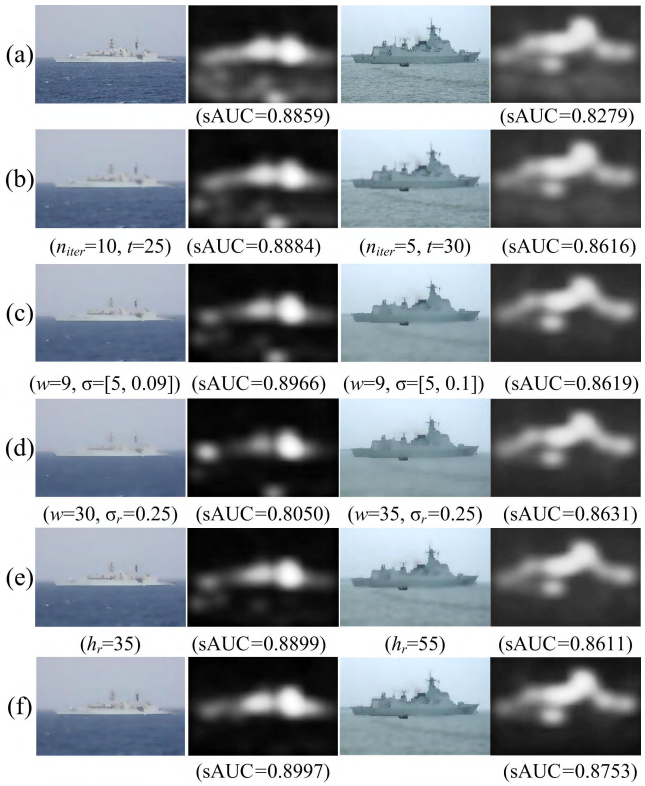

FIGURE 13. Visual image saliency detection results. Saliency map of: (a) The original visual images; (b) The smoothed results of the anisotropic diffusion filtering, (n_{iter}, t); (c) The smoothed results of the bilateral filtering, (w; σ); (d) The smoothed results of the propagation filtering, (w; σ_r); (e) The smoothed results of the mean shift filtering with fixed range bandwidth, (h_r); (f) The smoothed results of the proposed method.

works have been carried out for saliency detection [50]. A popular saliency detection method is the one called graph-based visual saliency [51]. This model can powerfully predict human fixations.

Fig. 12 and Fig. 13 show the saliency detection results of the IR and visual ship target images respectively. To evaluate the performance of saliency detection results using each filtered image, we apply the widely used shuffled Area Under the Curve (sAUC) metric [52]. For a perfect prediction, the sAUC equals 1.0, and any static saliency map will give a score of approximately 0.5. From Fig. 12 and Fig. 13 we note that ship target regions show high saliency in both IR and visual images, and with efficient image smoothing, it is helpful to suppress the backgrounds and enhance the saliency of ship target regions. By comparing with the other four methods in terms of the sAUC metric, we can see that the proposed method obtains the highest sAUC for both IR and visual images. Therefore, we verify that our adaptive mean shift filtering method can be applied to improve the performance of salient region detection. It is worth repeating that since our proposed method utilizes the distinguishing local properties of the ship targets and backgrounds, it adapts well to different images, and achieves a better ship target edge preservation smoothing output for both IR and visual images.

IV. CONCLUSION

In this paper, we propose a multi-modal ship target image smoothing method based on adaptive mean shift filtering. This method can effectively suppress the noises as well as preserve the ship target structures. First, based on the analysis of local region properties, we develop a block based ship target region detection method to distinguish the ship target region from the background region. This is important for preserving details of the ship target. Then, by associating the range bandwidth with local region properties of the IR and visual images, we propose an adaptive range bandwidth calculation method for mean shift filtering. Experimental results show that the proposed method works well for different IR and visual ship target images. It can effectively suppress complex background noises while preserving the details of ship targets. By comparing with four well-known edge-preserving denoising methods, including the anisotropic diffusion filtering, the bilateral filtering, the propagation filtering, and the mean shift filtering with fixed range bandwidth, comparison results demonstrate that the proposed method has superior performances, achieving higher average LCP-SI, EBMC, SMPI, and lower average ME and RAE. This is useful for improving the performance of various applications, such as ship target image segmentation and salient region detection.

ACKNOWLEDGMENT

We would like to thank our co-researchers for providing the image datasets. We are also grateful to our colleagues for their great help in constructing the ground truth, and to the anonymous reviewers and the editor for their valuable comments and suggestions which are very helpful in improving the quality of the paper. This paper has been presented in an International Conference [40].

REFERENCES

[1] K. Krapels, R. G. Driggers, and J. F. Garcia, "Performance of infrared systems in swimmer detection for maritime security," *Opt. Exp.*, vol. 15, no. 19, pp. 12296–12305, 2007.
[2] N. Rahmani and A. Behrad, "Automatic marine targets detection using features based on local Gabor binary pattern histogram sequence," in *Proc. 1st Int. eConf. Comput. Knowl. Eng. (ICCKE)*, Mashhad, Iran, 2011, pp. 195–201.
[3] Z. Liu, F. Zhou, X. Bai, and X. Yu, "Automatic detection of ship target and motion direction in visual images," *Int. J. Electron.*, vol. 100, no. 1, pp. 94–111, 2011.
[4] X. Bai, Z. Chen, Y. Zhang, Z. Liu, and Y. Lu, "Infrared ship target segmentation based on spatial information improved FCM," *IEEE Trans. Cybern.*, vol. 46, no. 12, pp. 3259–3271, Dec. 2016.
[5] A. Buades, B. Coll, and J.-M. Morel, "A review of image denoising algorithms, with a new one," *Multiscale Model. Simul.*, vol. 4, no. 2, pp. 1–41, 2005.
[6] P. Qiu and P. S. Mukherjee, "Edge structure preserving image denoising," *Signal Process.*, vol. 90, no. 10, pp. 2851–2862, 2010.
[7] P. Jain and V. Tyagi, "A survey of edge-preserving image denoising methods," *Inf. Syst. Frontiers*, vol. 18, no. 1, pp. 159–170, 2016.
[8] P. Jain and V. Tyagi, "LAPB: Locally adaptive patch-based wavelet domain edge-preserving image denoising," *Inf. Sci.*, vol. 294, no. 10, pp. 164–181, 2015.
[9] S. J. Ko and Y. H. Lee, "Center weighted median filters and their applications to image enhancement," *IEEE Trans. Circuits Syst.*, vol. 38, no. 9, pp. 984–993, Sep. 1991.
[10] P. Perona and J. Malik, "Scale-space and edge detection using anisotropic diffusion," *IEEE Trans. Pattern Anal. Mach. Intell.*, vol. 12, no. 7, pp. 629–639, Jul. 1990.

[11] Y. Wang, Y. Shao, Z. Gui, Q. Zhang, L. Yao, and Y. Liu, "A novel fractional-order differentiation model for low-dose CT image processing," *IEEE Access*, vol. 4, pp. 8487–8499, 2016.
[12] C. Tomasi and R. Manduchi, "Bilateral filtering for gray and color images," in *Proc. 6th Int. Conf. Comput. Vis.*, Bombay, India, 1998, pp. 839–846.
[13] D. Comaniciu and P. Meer, "Mean shift: A robust approach toward feature space analysis," *IEEE Trans. Pattern Anal. Mach. Intell.*, vol. 24, no. 5, pp. 603–619, May 2002.
[14] A. C. Bovik, T. S. Huang, and D. C. Munson, "The effect of median filtering on edge estimation and detection," *IEEE Trans. Pattern Anal. Mach. Intell.*, vol. PAMI-9, no. 2, pp. 181–194, Mar. 1987.
[15] Z. Wang and D. Zhang, "Progressive switching median filter for the removal of impulse noise from highly corrupted images," *IEEE Trans. Circuits Syst. II, Analog Digit. Signal Process.*, vol. 46, no. 1, pp. 78–80, Jan. 1999.
[16] V. V. Khryashchhev, A. L. Priorov, I. V. Apalkov, and P. S. Zvonarev, "Image denoising using adaptive switching median filter," in *Proc. IEEE Int. Conf. Image Process.*, Genoa, Italy, Sep. 2005, pp. 117–120.
[17] K. S. Srinivasan and D. Ebenezer, "A new fast and efficient decision-based algorithm for removal of high-density impulse noises," *IEEE Signal Process. Lett.*, vol. 14, no. 3, pp. 189–192, Mar. 2007.
[18] S. Shrestha, "Image denoising using new adaptive based median filter," *Signal Image Process., Int. J.*, vol. 5, no. 4, pp. 1–13, 2014.
[19] N. U. Khan, K. V. Arya, and M. Pattanaik, "Edge preservation of impulse noise filtered images by improved anisotropic diffusion," *Multimed. Tools Appl.*, vol. 73, no. 1, pp. 573–597, 2014.
[20] J. Xu, Y. Jia, Z. Shi, and K. Pang, "An improved anisotropic diffusion filter with semi-adaptive threshold for edge preservation," *Signal Process.*, vol. 119, pp. 80–91, Feb. 2016.
[21] K. N. Chaudhury, D. Sage, and M. Unser, "Fast $O(1)$ bilateral filtering using trigonometric range kernels," *IEEE Trans. Image Process.*, vol. 20, no. 12, pp. 3376–3382, Dec. 2011.
[22] Z. C. Wang, "A bilateral filtering based image de-noising algorithm for night time infrared monitoring images," in *Proc. Int. Conf. Comput. Sci. Comput. Intell.*, Las Vegas, NV, USA, 2014, pp. 199–203.
[23] K. He, J. Sun, and X. Tang, "Guided image filtering," *IEEE Trans. Pattern Anal. Mach. Intell.*, vol. 35, no. 6, pp. 1397–1409, Jun. 2013.
[24] Y. Yang, W. Wan, S. Huang, F. Yuan, S. Yang, and Y. Que, "Remote sensing image fusion based on adaptive IHS and multiscale guided filter," *IEEE Access*, vol. 4, pp. 4573–4582, 2016.
[25] J.-H. R. Chang and Y.-C. F. Wang, "Propagated image filtering," in *Proc. IEEE Conf. Comput. Vis. Pattern Recognit. (CVPR)*, Boston, MA, USA, 2015, pp. 10–18.
[26] L. I. Rudin, S. Osher, and E. Fatemi, "Nonlinear total variation based noise removal algorithms," *Phys. D, Nonlinear Phenom.*, vol. 60, nos. 1–4, pp. 259–268, 1992.
[27] H. Liu, J. Gu, M. Q. H. Meng, and W. S. Lu, "Fast weighted total variation regularization algorithm for blur identification and image restoration," *IEEE Access*, vol. 4, pp. 6792–6801, 2016.
[28] H. Liu, R. Xiong, S. Ma, X. Fan, and W. Gao, "Non-local extension of total variation regularization for image restoration," in *Proc. IEEE Int. Symp. Circuits Syst. (ISCAS)*, Melbourne, VIC, Australia, Jun. 2014, pp. 1102–1105.
[29] A. Buades, B. Coll, and J.-M. Morel, "A non-local algorithm for image denoising," in *Proc. IEEE Comput. Soc. Conf. Comput. Vis. Pattern Recognit.*, vol. 2. San Diego, CA, USA, Jun. 2005, pp. 60–65.
[30] M. Lebrun, A. Buades, and J.-M. Morel, "A nonlocal Bayesian image denoising algorithm," *SIAM J. Imag. Sci.*, vol. 6, no. 3, pp. 1665–1688, 2013.
[31] V. Fedorov and C. Ballester, "Affine non-local means image denoising," *IEEE Trans. Image Process.*, vol. 26, no. 5, pp. 2137–2148, May 2017.
[32] W. Tao and H. Jin, "Unified mean shift segmentation and graph region merging algorithm for infrared ship target segmentation," *Opt. Eng.*, vol. 46, no. 12, p. 127002, 2007.
[33] W. Liu, Y. Duan, K. Shao, and L. Zhang, "Image smoothing based on the mean shift algorithm," in *Proc. IEEE Int. Conf. Control Autom.*, Jun. 2007, pp. 1349–1353.
[34] B. Park and J. S. Marron, "Comparison of data-driven bandwidth selectors," *J. Amer. Statist. Assoc.*, vol. 85, no. 409, pp. 66–72, 1990.
[35] S. J. Sheather and M. C. Jones, "A reliable data-based bandwidth selection method for kernel density estimation," *J. Roy. Statist. Soc. B*, vol. 53, no. 3, pp. 683–690, 1991.
[36] J. E. Chacón, T. Duong, and M. P. Wand, "Asymptotics for general multivariate kernel density derivative estimators," *Statist. Sinica*, vol. 21, no. 2, pp. 807–840, 2011.
[37] J. E. Chacón and T. Duong, "Bandwidth selection for multivariate density derivative estimation, with applications to clustering and bump hunting," *Electron. J. Statist.*, vol. 7, pp. 499–532, Apr. 2013.
[38] J. E. Chacón and P. Monfort. (2013). "A comparison of bandwidth selectors for mean shift clustering." [Online]. Available: https://arxiv.org/abs/1310.7855
[39] D. Comaniciu, "An algorithm for data-driven bandwidth selection," *IEEE Trans. Pattern Anal. Mach. Intell.*, vol. 25, no. 2, pp. 281–288, Feb. 2003.
[40] Z. Liu, C. Sun, X. Bai, and F. Zhou, "Infrared ship target image smoothing based on adaptive mean shift," in *Proc. Int. Conf. Digit. Image Comput., Techn. Appl. (DICTA)*, Wollongong, NSW, Australia, Nov. 2014, pp. 1–8.
[41] H.-H. Yeh and C.-S. Chen, "From rareness to compactness: Contrast-aware image saliency detection," in *Proc. IEEE Int. Conf. Image Process.*, Bangalore, India, 2012, pp. 1077–1080.
[42] Q. Luo and T. M. Khoshgoftaar, "Efficient image segmentation by mean shift clustering and MDL-guided region merging," in *Proc. IEEE Int. Conf. Tools Artif. Intell.*, Boca Raton, FL, USA, Nov. 2004, pp. 337–343.
[43] R. A. Jayashree, "RGB to HSI color space conversion via MACT algorithm," in *Proc. Int. Conf. Commun. Signal Process. (ICCSP)*, Melmaruvathur, India, Apr. 2013, pp. 561–565.
[44] R. Hassen, Z. Wang, and M. M. A. Salama, "Image sharpness assessment based on local phase coherence," *IEEE Trans. Image Process.*, vol. 22, no. 7, pp. 2798–2810, Jul. 2013.
[45] A. Beghdadi and A. Le Negrate, "Contrast enhancement technique based on local detection of edges," *Comput. Vis. Graph.*, vol. 46, no. 2, pp. 162–174, 1989.
[46] Y. M. M. Babu, M. V. Subramanyam, and M. N. G. Prasad, "A survey on de-speckling of SAR images," *Int. J. Electron. Commun. Tech.*, vol. 5, no. 18, pp. 142–144, 2014.
[47] L. Sun and D. Y. Bi, "The improved iterative algorithm based on entropy for image threshold segmentation," (in Chinese), *Comput. Appl. Softw.*, vol. 25, no. 10, pp. 225–227, 2008.
[48] L. Grady, "Random walks for image segmentation," *IEEE Trans. Pattern Anal. Mach. Intell.*, vol. 28, no. 11, pp. 1768–1783, Nov. 2006.
[49] M. Sezgin and B. Sankur, "Survey over image thresholding techniques and quantitative performance evaluation," *J. Electron. Imag.*, vol. 13, no. 1, pp. 146–168, 2004.
[50] A. Borji, D. N. Sihite, and L. Itti, "Salient object detection: A benchmark," in *Proc. 12th Eur. Conf. Comput. Vis. (ECCV)*, Florence, Italy, 2012, pp. 414–429.
[51] J. Harel, C. Koch, and P. Perona, "Graph-based visual saliency," in *Proc. Adv. Neural Inf. Process. Syst.*, 2006, pp. 545–552.
[52] N. Riche, M. Duvinage, M. Mancas, B. Gosselin, and T. Dutoit, "Saliency and human fixations: State-of-the-art and study of comparison metrics," in *Proc. IEEE Int. Conf. Comput. Vis.*, Dec. 2013, pp. 1153–1160.

ZHAOYING LIU received the B.S. degree from Shandong University in 2007, and the Ph.D. degree from the Beijing University of Aeronautics and Astronautics, in 2015. She is currently a Post-Doctoral Researcher with the College of Computer Science, Beijing University of Technology. Her research interests include image segmentation, image registration, and object recognition.

XIANGZHI BAI received the B.S. degree in engineering and the Ph.D. degree in pattern recognition and intelligent system from the Beijing University of Aeronautics and Astronautics (BUAA), Beijing, China, in 2003 and 2009, respectively. He is currently an Associate Professor with the Image Processing Center, BUAA. He holds seven national invention patents and has published over 100 international journal and conference papers in the field of mathematical morphology, image analysis, pattern recognition, and bioinformatics. He also acts as an Active Reviewer for over 40 international journals and conferences.

CHANGMING SUN received the Ph.D. degree in computer vision from the Imperial College London, London, U.K., in 1992. He then joined CSIRO, Sydney, NSW, Australia, where he is currently a Principal Research Scientist carrying out research and involved on applied projects. His current research interests include computer vision, image analysis, and pattern recognition. He has served on the program/organizing committees of various international conferences. He is an Associate Editor of the EURASIP Journal on Image and Video Processing. He is a member of the Australian Pattern Recognition Society.

FUGEN ZHOU received the B.S. degree in electronic engineering and the M.S. and Ph.D. degrees in pattern recognition and intelligent systems from the Beijing University of Aeronautics and Astronautics, Beijing, China, in 1986, 1989, and 2006, respectively. His research interests include target detection and recognition, multimodality image processing, and biomedical image processing and recognition.

YUJIAN LI received the B.S. degree from the Department of Applied Mathematics, Huazhong University of Science and Technology, in 1990, and the M.S. and Ph.D. degrees from the Institute of Mathematics, Chinese Academy of Sciences and the Institute of Semiconductors, Chinese Academy of Sciences, in 1993 and in 1999, respectively. From 1993 to 1996, he was with the Institute of Biophysics of the Chinese Academy of Sciences. From 1999 to 2001, he was a Post-Doctoral Fellow at the Beijing University of Posts and Telecommunications. He has been a Professor with the College of Computer Science in the Beijing University of Technology, since 2001. His current research interests include image processing, pattern analysis, deep learning, and machine intelligence.